Hindawi
Shock and Vibration
Volume 2024, Article ID 5571578, 18 pages
https://doi.org/10.1155/2024/5571578

Research Article

TVMS Calculation and Dynamic Analysis of Cracked Gear considering Oil Film Stiffness

Jiateng Wu, Zhenqi Du, and Chengbiao Tong

College of Mechanical and Electrical Engineering, Hunan Agricultural University, Changsha 410128, China

Correspondence should be addressed to Jiateng Wu; jiat_wu@126.com

Received 6 November 2023; Revised 20 February 2024; Accepted 13 March 2024; Published 27 March 2024

Academic Editor: Sundararajan Natarajan

A time-varying meshing stiffness (TVMS) model that includes oil film stiffness in the elastohydrodynamic lubrication (EHL) line contact is proposed for tooth root cracking. This model employs the oil film thickness to estimate the stiffness of the oil film in gear contact by considering the profile variation of the oil film induced by tooth root cracks, to provide the evolution principle of TVMS in EHL line contact to study the effects of oil film stiffness of cracked gear on the TVMS. The results of the analysis reveal that the overall result of TVMS decreases owing to the stiffness of the oil film, whereas the combined TVMS depends mainly on the rotation speed of the gear system because the thickness of the oil film in the tooth crack is affected by the velocity of the entrainment. Furthermore, a six-degree-of-freedom (DOF) dynamic model is introduced to analyze the vibration behavior of the gear system using the combined TVMS results for different crack levels, and the influence of the combined TVMS on the vibration response of the tooth root crack is exhibited from the time-domain analysis, frequency-domain analysis, and statistical indicator analysis.

1. Introduction

As an important mechanical part, the gear is like "muscles and bones" in the structure of the human body, which cannot be seen or touched from the appearance, but it greatly affects the normal operation of machinery. The gear crack fault as an early failure state of the gear system is the main research point of the gear failure mechanism study. Although the theory of gear fault diagnosis has been improved, resulting in the cracked gear with more accuracy, it is necessary to have a better understanding of the vibration features of the cracked gear. In recent year, gear failure mechanism research, whose method is based on the model, has been used to reflect the influence of the dynamic parameter on the gear system.

In the model-based method, the time-varying meshing stiffness (TVMS), which is the primary excitation characteristic parameter, can affect the mechanism variation of the vibration signal in the dynamic model of the gear system and can be used as an important role in the diagnosis of gear failure [1]. Therefore, whether TVMS can be calculated accurately is one of the important links to reflect the failure mechanism of the gear system, and it is essential to evaluate the condition of the gear teeth to ensure normal operation of the gear system. Currently, researchers have carried out the TVMS estimation of gear system using the analytical method (AM) [2], the finite element model (FEM) [3], and the measurement-based method.

In AM, the meshing stiffness of line contact is often derived from the stiffness of Hertzian contact, the stiffness of the flexible base, the bending stiffness, and the shear stiffness, and the gear contact model is simulated by assuming the gear tooth as a half-section non-uniform cantilever beam [4–6]. Based on the results of the exploratory study, Kumar et al. [7] proposed a mathematical formulation of a pair of carburized spur gears that included the cracked tooth root for TVMS calculation through the AM. Shen et al. [8] present a modified TVMS analytical model to assess the influence of the depth of tooth wear by adopting Archard's wear equation [9]. Wang et al. [10] modify the coefficient and transition curve to revise the analytical model of TVMS for profile-shifted spur gears. Wu et al. [11] proposed an advanced method to correct foundation stiffness errors and take into consideration the influence of axial mesh forces to evaluate TVMS of helical gears with tooth spalls with curved bottom features. Woo-jin Chung et al. [12] developed a profile model of a trochoidal root profile using a virtual rack reflecting the cutter information to calculate TVMS and load static transmission error (LSTE) of the helical gear pair. Yang et al. [13] introduced a new term, which called torsional stiffness, into the overall TVMS and proposed an improved tooth tip chipping model to calculate the TVMS for gear tooth chipping defects.

The FEM method usually builds the gear pairs using a 3-D model and applies the load torque to the teeth to evaluate the TVMS throughout the meshing circle [14]. Zhan et al. [15] developed a new FE model, which contains NX, ANSYS-workbench, and quasistatic algorithm, to determine the TVMS of gear system. Verma et al. [16] determined the TVMS and tooth cracked propagation using extended the finite element method (XFEM), and XFEM can provide significant information to effectively define the discontinuity caused by faults like teeth cracks, etc. Sun et al. [17] recommend a revised TVMS model of gear pair, which relieves the tooth tip and lead crowning, and the proposed model is an improved TVMS result precision based on the slice method in FEM. The FEM method can quite estimate an exact TVMS result [18, 19], and its flexibility makes it convenient to model a gear tooth with different failure types [20], but every tooth needs to be modeled and especially the model mesh needs to be refined when the geometry of the gear system changes in FEM, making program codes more complicated [21] and time consuming [22].

In addition to the AM and FEM methods, some investigators indirectly obtain the TVMS of the gear system by using a measurement-based method. For example, the stress distribution of a visual structure during the gear system meshing circle is obtained with the help of a photoelastic measuring device [23] and evaluates the TVMS of the gear pair. Patil et al. [24] design a special test rig for measuring the single-tooth stiffness of involute spur gear experimentally and proposed an experimental technique to estimate the influence of the pressure angle on the pinion side on the stiffness of the mesh. Different stress-strain collection devices are used to measure the load at the root of the contact gear pair [25], and the TVMS of the gear system is calculated indirectly. However, the measurement-based method does not always provide results that show good effectiveness with other methods, especially for the existing problem with the harsh conditions of experimental measurement and the particularity of gear materials [26].

At the same time, with the development of the dynamic mechanism of gear contact, the elastohydrodynamic lubrication theory (EHL) and the dynamic properties of oil film including lubrication in the gear meshing have begun to become a major focus of the researchers. Wen et al. study the resulting stiffness in the EHL model by introducing the normal stiffness of the oil film to analyze the thickness of the film and elastic deformation [27]. Zhang et al. show strong nonlinearity and the time-varying feature of the stiffness of cylindrical roller bearings when considering the performance of oil lubrication [28]. Zhang et al. proposed an EHL tribo-vibration model to analyze the normal stiffness of the oil film in the EHL contact area [29], and the effects of normal load, rolling speed, and amplitude of regular surface waviness on the stiffness of the oil film are estimated [30]. Zhou et al. investigate the normal and tangential stiffness of the oil film under various geometries of the gear pair and working conditions [31], while the novel oil film model is developed in both normal and tangential directions to contain the stiffness of the oil film [32].

Although the dynamic of cracked gears has been developed extensively to predict the vibration analysis for gear fault diagnosis, previous investigations on the failure mechanism of gears focus on the contact stiffness or cracked gear model and lacked the TVMS estimation of cracked gear under theoretical EHL models. Therefore, the meshing stiffness of the cracked gear consisting of EHL is carried out to construct an improved TVMS evaluation method, to provide the evolution principle of TVMS in the contact of the EHL line, and to present an effective dynamic parameter of vibration analysis for the diagnosis of failure of the cracked gear in this paper.

(i) An analytical TVMS model is developed for gear contact EHL, in which the meshing stiffness of the EHL model is introduced to reflect the TVMS variation due to the crack of the tooth root.

(ii) With the developed model, the impact of the EHL model on cracked tooth is investigated. A six-degree-of-freedom (DOF) dynamic model of the gear system is produced including the 4-translation DOF and 2-rotation DOF for the gear pair.

(iii) The vibration behaviors of the dynamic response under the different levels of cracked tooth, which are obtained from the TVMS of the EHL model, are studied, and the influence of TVMS due to the contact of the EHL line on the vibration response of cracked tooth is exhibited.

2. Methods

The meshing stiffness of gear contact is used to describe the ability of the gear to resist deformation under an alternating load. Since the rotation of teeth affects the contact position of gear, hence the meshing stiffness becomes a function of time, namely time-varying meshing stiffness, and that also describes the vibration characteristic of the gear pair. Since the existence of cracks will change the geometry and eventually affect the TVMS, the TVMS plays an important role in the fault analysis of dynamic modeling.

To present the generality of the gear model, Figure 1 shows the schematic diagram of a nonuniform cantilever beam of spur gear. As for AM, the tooth section is divided into **n** segments to analyze the deformation principle, and the total deformation of contact gear δ includes kinds of component: bending, shear, axis, and Hertzian contact. Correspondingly, the meshing stiffness can be derived:

bending stiffness K_b, shear stiffness K_s, axis compressive stiffness K_a, fillet foundational stiffness K_f, and Hertzian stiffness K_h.

2.1. Tooth Stiffness (K_b, K_s *and* K_a) *by using the Potential Energy Method.* Potential energies stored of bending, shear, and axis compressive deformation in the meshing contact can be expressed respectively as follows:

$$U_b = \frac{F_b^2}{2K_b}, \tag{1}$$

$$U_s = \frac{F_s^2}{2K_s}, \tag{2}$$

$$U_a = \frac{F_a^2}{2K_a}. \tag{3}$$

Based on the nonuniform cantilever beam theory [4], the energies of bending, shear, and compressive axis comprises an involute and transitional part as follows:

$$U_b = \int_{y_1}^{y_2} \frac{M_1^2}{2\mathrm{EI}_y}\mathrm{d}y + \int_{y_2}^{y_3} \frac{M_2^2}{2\mathrm{EI}_y}\mathrm{d}y, \tag{4}$$

$$U_s = \int_{y_1}^{y_2} \frac{1.2F_b^2}{2\mathrm{GA}_y}\mathrm{d}y + \int_{y_2}^{y_3} \frac{1.2F_b^2}{2\mathrm{GA}_y}\mathrm{d}y, \tag{5}$$

$$U_a = \int_{y_1}^{y_2} \frac{F_a^2}{2\mathrm{EA}_y}\mathrm{d}y + \int_{y_2}^{y_3} \frac{F_a^2}{2\mathrm{EA}_y}\mathrm{d}y, \tag{6}$$

where the $M_{1,2}$ and $F_{a,b}$ are the bending moment of 1, 2 tooth and the contact force components of axial compressive and bending on the tooth, respectively, E and G are the modulus of elasticity and shear. Then the expression combining of equations (1)–(3) and (4)–(6), the stiffness of bending, axis, and shear can be described as follows [19]:

$$\begin{aligned}
K_b &= \int_{\pi/2}^{\gamma_1} \frac{[\cos\beta(y_3 - y) - x_3\sin\beta]^2}{\mathrm{EI}_y}\frac{\mathrm{d}y}{\mathrm{d}\gamma}\mathrm{d}\gamma + \int_{\tau_b}^{\beta} \frac{[\cos\beta(y_3 - y) - x_3\sin\beta]^2}{\mathrm{EI}_y}\frac{\mathrm{d}y}{\mathrm{d}\tau}\mathrm{d}\tau,\\
K_s &= \int_{\pi/2}^{\gamma} \frac{1.2\cos^2\beta}{\mathrm{GA}_y}\frac{\mathrm{d}y}{\mathrm{d}\gamma}\mathrm{d}\gamma + \int_{\tau_b}^{\beta} \frac{1.2\cos^2\beta}{\mathrm{GA}_y}\frac{\mathrm{d}y}{\mathrm{d}\gamma}\mathrm{d}\gamma,\\
K_a &= \int_{\pi/2}^{\gamma} \frac{\sin^2\beta}{\mathrm{EA}_y}\frac{\mathrm{d}y}{\mathrm{d}\gamma}\mathrm{d}\gamma + \int_{\tau_b}^{\beta} \frac{\sin^2\beta}{\mathrm{EA}_y}\frac{\mathrm{d}y}{\mathrm{d}\gamma}\mathrm{d}\gamma.
\end{aligned} \tag{7}$$

The single-tooth stiffness based on the potential energy method can be calculated as follows:

$$\frac{1}{K_t} = \frac{1}{K_b} + \frac{1}{K_s} + \frac{1}{K_a}. \tag{8}$$

2.2. Fillet-Foundation Stiffness (K_f) *and Hertzian Contact Stiffness* (K_h). As the tooth is supported by the contact load, the deflection of the fillet foundation also influences the TVMS on the gear pair, which is provided to alleviate the stress concentration at the root of the tooth. According to Muskhelishvili's theory [4], the stiffness of the fillet foundation is calculated to apply the single-tooth engagement. However, the structural coupling effects caused by different teeth engaged are different when double-teeth contact, and the value of single-tooth engagement is overestimated because the contacting teeth share the same gear body. Therefore, the analytical formulas of double-teeth proposed by Reference [7] are introduced to evaluate the stiffness of the foundation of the gear fillet.

The stiffness of the fillet foundation of single-tooth engagement can be described as follows:

$$\frac{1}{K_{fs}} = \frac{\cos^2\alpha_m}{\mathrm{EW}}\left\{L^*\left(\frac{u_f}{s_f}\right)^2 + M^*\left(\frac{u_f}{s_f}\right) + P^*\left(1 + Q^*\tan^2\alpha_m\right)\right\} \quad \text{Single tooth contact}, \tag{9}$$

where the special coefficients which are developed by polynomial functions, such as L^*, M^*, P^*, and Q^*, can be given by

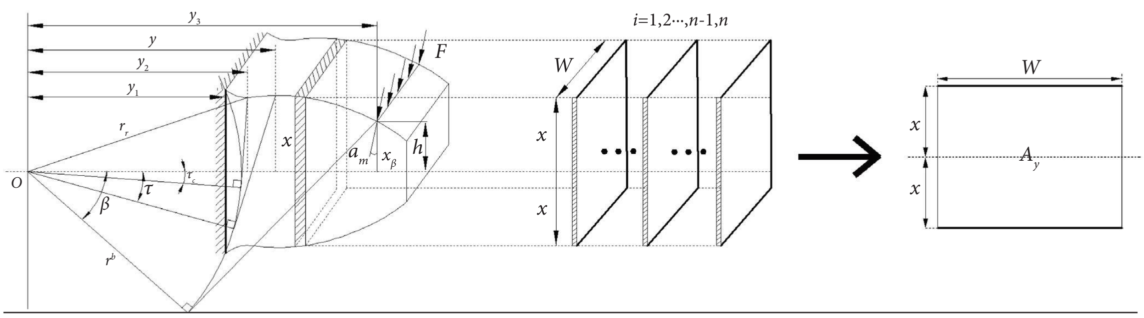

Figure 1: Model of a nonuniform cantilever beam of spur gear.

$$X_i^*\left(h_{fi},\theta_f\right)=\frac{A_i}{\theta_f^3}+B_ih_{fi}^2+\frac{C_i}{\theta_f^2}+D_ih_{fi}^2+E_i\frac{h_{fi}^2}{\theta_f}+F_i\frac{h_{fi}}{\theta_f}+G_i\frac{h_{fi}}{\theta_f^2}+H_ih_{fi}+I_i, \tag{10}$$

$$X_i^*\left(h_{fi},\theta_f\right)=A_i\theta_f^3+\frac{B_i}{h_{fi}^3}+C_i\theta_f^2+\frac{D_i}{h_{fi}^2}+E_i\frac{\theta_f}{h_{fi}^2}+F_i\frac{\theta_f}{h_{fi}}+G_i\frac{\theta_f^2}{h_{fi}}+\frac{H_i}{h_{fi}}+I_i, \tag{11}$$

$$h_{fi}=\frac{r_f}{r_{\text{int}}}, \tag{12}$$

where the θ_f and r_f represent arc angle of half-tooth and the radius of the root circle, respectively, and r_{int} is the inner radius of tooth. The Q^* is calculated by equation (10) and L^*, M^*, and P^* are calculated by (11), where coefficients of A_i, B_i, C_i, D_i, E_i, F_i, G_i, H_i, and I_i are obtain in Reference [5].

The fillet-foundation stiffness of double-tooth engagement with structural coupling effects can be given by:

$$\frac{1}{K_{\text{fd}}}=\frac{\cos^2\alpha_1\cos^2\alpha_2}{\text{EW}}\left\{L^*\left(\frac{u_1u_2}{s_f}\right)^2+\left(M^*\tan\alpha_2+P^*\right)\left(\frac{u_1}{s_f}\right)+,\ldots,+\left(Q^*\tan\alpha_1+R^*\right)\left(\frac{u_2}{s_f}\right)+\left(S^*\tan\alpha_1+T^*\right)\tan\alpha_2\right.$$
$$\left.+U^*\tan\alpha_1+V^*\right\}\text{Double tooth contact}, \tag{13}$$

where the coefficients of L^*, M^*, P^*, Q^*, R^*, S^*, T^*, U^* and V^* are fitted by polynomial functions with (10) and (11). The L^*, P^*, R^*, S^* and V^* are obtained by (10) and the M^*, Q^*, T^* and U^* are obtained by (11).

In addition, Hertzian contact stiffness is used to define the deformations from the contact field of gear pairs, and contact deformation is generally described as a non-linear variation by considering tooth modification [17]. Therefore, the non-linear Hertzian contact stiffness can be given as:

$$K_h=\frac{E^{0.9}L^{0.8}F_i^{0.1}}{1.275}, \tag{14}$$

where $F_i=F\cdot\text{LSR}_i$ and the LSR_i is the load share ratio of the ith tooth, which has a flow chart in Ref. [17] is to analyze the non-linear process of gear contact.

2.3. Stiffness of the Oil Film (K_{oil}). In general, the gear pair contact process is carried out in the lubrication state, that is, the contact position of the tooth surface includes micro convex body contact and oil film contact [31]. The stiffness of the oil film is essential for the dynamic modeling of the gear system with regard to the hydrodynamic effect of the lubricant [33]. Therefore, the gear contact of the tooth surface with lubrication effect must be considered by using the EHL model. The EHL model is widely used to analyze the gear pair contact problem considering the analysis of lubricating oil film thickness, contact pressure, oil viscosity, surface roughness, entrainment rate, effective contact area, and film shear stress.

For the line lubrication of the gear contact, the EHL model at any meshing angle of tooth contact can be given as [34]:

$$\begin{cases} \dfrac{\partial}{\partial x}\left[s_0\left(\dfrac{P_h b}{12\nu_0 u}\right)\left(\dfrac{\overline{\rho h}^3}{\overline{\nu}}\right)\dfrac{\partial p}{\partial x}\right] = \dfrac{\partial}{\partial x}(\overline{\rho h}) + \dfrac{\partial}{\partial \overline{t}}(\overline{\rho h}), \\ \overline{w} = \displaystyle\int_{x_{\text{in}}}^{x_{\text{out}}} \left[p(x,\overline{t}) + p_c(x,\overline{t})\right]\mathrm{d}x, \\ \overline{h} = \dfrac{h_0}{b} + \left(\dfrac{b}{2R}\right)x^2 + \dfrac{\delta(x,\overline{t})}{b} + S(x,\overline{t}), \end{cases} \tag{15}$$

where coefficient b is half width of Hertzian contact, $\overline{h}$ is the dimensionless equation of oil film thickness, P_h is the maximum pressure of Hertzian contact, u denote surface sliding velocities of the surface of the lubricating oil on contact bodies, $\overline{t}$ denote the function of dimensionless time and can be written as $\overline{t} = ut/b$, and the dimensionless parameters mentioned above are standardized by using half width b. s_0 is the non-Newtonian lubricant function based on the ultimate shear stress, oil pressure and oil viscosity of tooth surface, h_0 is the central film thickness, R is the equivalent radius of curvature, $\delta(x,\overline{t})$ is the total elastic deformation of contact surface, $S(x,\overline{t})$ is the composite function of surface roughness, $\overline{w}$ is dimensionless load of per unit surface, x_{out} and x_{in} are the dimensionless coordinates of the inlet and outlet contact position, p_c is the contact pressure of roughness surface. $\overline{\nu}$ and $\overline{\rho}$ are presents dimensionless oil viscosity and oil density which are the function of contact pressure and can be determined as:

$$\begin{cases} \overline{\nu} = \nu_0 \exp\left\{(\ln \nu_0 + 9.67)\left[\left(1 + 5.1\times 10^{-9}\cdot p\right)^z\left(\dfrac{T-138}{T_0-138}\right)^{-q} - 1\right]\right\}, \\ \overline{\rho} = \rho_0\left[1 + \dfrac{0.6\times 10^{-9}P_h}{1+1.7\times 10^{-9}P_h} - 6.5\times 10^{-4}(T-T_0)\right], \end{cases} \tag{16}$$

where T_0, ν_0 and ρ_0 are the temperature, lubricant viscosity and lubricant density at ambient pressure, respectively.

The gear contact of the EHL line can be determined as the model between an elastic body with a comprehensive curvature radius and a rigid flat. The elastic deformation of the oil film generally occurs within the normal contact field of the gear pair under the rated lubricant pressure-viscosity relation and the oil film between the contact field of elastic bodies is equivalent to a minimal mass of spring element as shown in Figure 2, where $k_1, k_2, \ldots,$ and k_n, represent contact stiffness of normal rigid, the k_{oil} is the contact stiffness of oil film. In the EHL line contact, the oil film pressure $p(x,t)$ and oil film thickness $h(x,t)$ are calculated by using (15). In addition, the contact stiffness of the oil film, including the increase contact force effect, can be defined as follows [31]:

$$K_{\text{oil}} = \frac{\Delta F_n(t)}{\Delta x_n(t)} = b\cdot\Delta x(t)\sum_{i=1}^{n}\frac{\Delta p(x,t)}{\Delta h(x,t)}, \tag{17}$$

where b is the contact width, Δ is increment, $x(t)$ refers to the meshing position along the direction-x.

Based on the above stiffness calculation, the overall meshing stiffness for the gear pairs can be estimated by

$$K = \begin{cases} \dfrac{1}{\left(1/K_t + 1/K_{fs} + 1/K_h + 1/K_{\text{oil}}\right)} & \text{Single tooth contact,} \\ \displaystyle\sum_{i=1}^{2}\dfrac{1}{\left(1/K_{t,i} + 1/K_{fd,i} + 1/K_{h,i} + 1/K_{\text{oil},i}\right)} & \text{Double tooth contact,} \end{cases} \tag{18}$$

where the subscript i represents the ith meshing gear teeth.

2.4. Modeling TVMS of Tooth Crack by considering Oil Film Stiffness.

In this section, an EHL line contact model is utilized to evaluate the TVMS of oil film under the cracked gear. In this model, the oil film thickness is employed to calculate the elastic deformation of the oil film by considering the variation trend of the oil film thickness with the crack of the tooth root because the profile variation of the oil film induced by the cracked tooth is involved in TVMS. Ma et al. [19] consider three different crack propagations of the tooth root, and the 2^{nd} and 3^{nd} methods are more close to the FEM results, so this paper adopts the second method for crack modeling in gear contact with the same assumptions. Figure 3 describes the schematic of a cross-section crack at the root of the tooth with constant depth q. In addition, the cross-sectional area A_y and inertia moment area I_y are vary as the root crack happened, respectively, which can be corrected as follows:

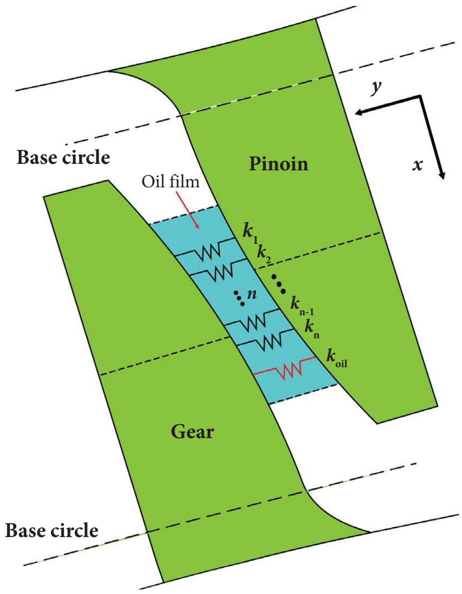

FIGURE 2: Schematic of gear contact with EHL film.

When $q = q_1 < q_{\max}$

$$I_y = \begin{cases} \dfrac{1}{12}(2x)^3 L, & y \le y_{c1}, \\ \dfrac{1}{12}\left[\dfrac{x_\beta - x_{c1}}{\left(y_\beta - y_{c1}\right)^2}(y - y_{c1})^2 + x_{c1} + x\right]^3 L, & y > y_{c1}, \end{cases}$$

$$A_y = \begin{cases} 2xL, & y \le y_{c1}, \\ \left[\dfrac{x_\beta - x_{c1}}{\left(y_\beta - y_{c1}\right)^2}(y - y_{c1})^2 + x_{c1} + x\right] L, & y > y_{c1}, \end{cases} \quad (19)$$

when $q = q_{1\max} + q_2$

$$I_y = \begin{cases} \dfrac{1}{12}(2x)^3 L, & y \le y_{c1}, \\ \left[\dfrac{x_\beta - x_{c1}}{\left(y_\beta - y_{c1}\right)^2}(y - y_{c1})^2 + x_{c1} + x\right] L, & y_{\max} \le y \le y_{c1}, \\ \dfrac{1}{12}\left[\dfrac{x_\beta + x_{c1}}{\left(y_\beta - y_{c1}\right)^2}(y - y_{c1})^2 - x_{c1} + x\right]^3 L, & y > y_{c1}, \end{cases}$$

$$A_y = \begin{cases} 2xL, & y \le y_{c1}, \\ \left[x - \dfrac{(y - y_{\max})x_{c1}}{y_{c1} - y_{\max}}\right] L, & y_{\max} \le y \le y_{c1}, \\ \left[\dfrac{x_\beta + x_{c1}}{\left(y_\beta - y_{c1}\right)^2}(y - y_{c1})^2 - x_{c1} + x\right] L, & y > y_{c1}. \end{cases} \quad (20)$$

For the pair of gears with EHL contact, the elastic contact between the gears is made in contact with the rigid plane by an elastic cylinder with the equivalent radius of curvature R and the elastic modulus E, as shown in Figure 4. The thickness of the oil film in the contact position will modify as the tooth surface elastically deforms due to cracked roots. Also, the elastic deformation of the tooth surface for the calculation of the stiffness of the oil film is still affected by cracked tooth root.

To evaluate the variation in the stiffness of the oil film under the root crack, the elastic deformation of the tooth surface is investigated under a uniform linear load. As seen in Figure 5, the shadow of the slash is the deformation of the tooth surface caused by the root crack, which defined as $\Delta\delta$, and the normal displacement of each contact point for the linear area load of compressive stress P and width ds applying the theory of EHL in (15) can be expressed as follows:

$$\delta(x, y) = \frac{p\mathrm{ds}}{\pi}\left\{c_1\left[\ln\left[(x - s)^2 + y^2\right] - \frac{y^2}{(x - s)^2 + y_2}\right] - c_2\frac{(x - s)^2}{(x - s)^2 + y^2}\right\} + C. \quad (21)$$

As the lubricant flows through the contact domain of gear pairs, the normal displacement of the oil film is caused by contact bending and Hertzian deformation, as given in (7), (14), and (15). Thus, the deformation of oil film $\Delta\delta$ under tooth root crack in (21) can be written as follows:

$$\Delta\delta = \delta_H + \delta_b. \quad (22)$$

Therefore, the dimensionless equation of oil thickness in (15) under the tooth root crack is $\overline{h}(\Delta\delta, t)$, and the mesh stiffness of the oil film in (17) can be expressed as follows:

$$K_{\mathrm{oil,crack}} = b \cdot \Delta\delta(t)\sum_{i=1}^{n}\frac{\Delta p(x, t)}{\Delta h(\Delta\delta, t)}. \quad (23)$$

Given by (18) and (23), the total TVMS of the cracked gear can be expressed as follows:

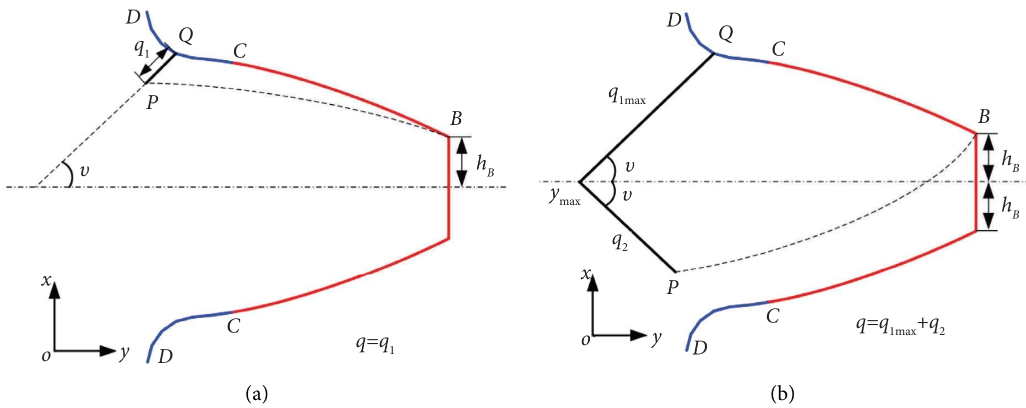

Figure 3: Schematic of crack propagation in Ma et al. [19]: (a) $q \le q_{1\,\max}$, (b) $q \ge q_{1\,\max}$.

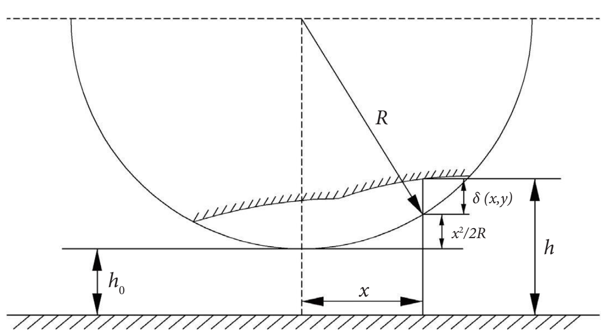

Figure 4: Line contact model of oil film.

$$K = \frac{1}{\left(1/K_n + 1/K_c\right)}. \tag{24}$$

3. Results Analysis for TVMS Calculation

In this section, a mathematical model of the pair of gears is used to compare with the AM method to understand the effect of the proposed method on the oil film stiffness of TVMS under cracked gear. The research framework is shown in Figure 6. The parameters of the calculated gear pair are given in Table 1. The overall time of teeth meshing is taken as the angle of the circle, $\theta = 17$. Figure 7 illustrates the results of TVMS based on the health gear between the AM and proposed method, and to compare with AM, and proposed method, ISO-6336-1-2006 is introduced for demonstrating the error criterion of two methods in Table 2.

From Figure 7 and Table 2, the TVMS result obtained in the proposed method is lower than that of the TVMS of the AM and FEM methods in both the double-contact meshing area and the single-contact meshing area. The differences between the proposed method and AM under the maximum stiffness of single contact and the average stiffness of total meshing are 0.9409×10^8 (N/m) and 1.6987×10^8 (N/m), respectively. For the same comparative content, the differences between the proposed method and FEM are the 1.0562×10^8 (N/m) and 1.5623×10^8 (N/m). It is indicated that the overall meshing stiffness results of the proposed method decrease compared to AM and FEM because the oil film stiffness is considered in the meshing stiffness calculation for healthy gear. Also, we can find that the result of proposed method is more close to the ISO, and the relative errors that contain the maximum stiffness of single contact and the average stiffness of total meshing are 3.12% and 9.51%, respectively.

The overall stiffness of the meshing that varies with the contact force along the line of action (LOA) is calculated. Figure 8 designates the relative results of the TVMS when the contact forces are 100, 200, 300, 400, and 500 KN/m. From Figure 8, it can be found that the increment of TVMS is increased with the continuous increase of contact force, and the increasing TVMS in the double-tooth contact area is more than the single-tooth contact area of TVMS.

The curve of TVMS variation under different speed increments along LOA is shown in Figure 9. As the rotation speed increases, the oil entrainment velocity between the contact surface increases as the pinion rotation speed increases, simultaneously increasing the oil film thickness and decreasing the oil film stiffness. The reason for this result is that the normal stiffness of the elastic contact is independent of the entrainment velocity, which remains constant with increasing speed. From Figure 9, it is found that with the rotation speed of pinion increases, the reduction rate of TVMS in the double-contact region is greater than that in the single-contact region, and with the continuous increase of rotation speed, the varying rate of TVMS is significantly reduced. Furthermore, to calculate the TVMS of the cracked root along the entire width of the tooth under a meshing cycle, the crack angle is set as α_c from Reference [7], and the crack depths are laid out with three constants expressed as 0.5 mm, 1.0 mm, and 1.5 mm. The TVMS with three crack depths is obtained by (24), as shown in Figure 10, and it is clearly shown that the TVMS result is rapidly decreased in the fully meshing region when the crack depth of the tooth root increases.

As seen in Figure 11, the double-tooth meshing region and the single-tooth meshing region are enlarged to compare the TVMS results of the cracked root under the EHL contact calculation. Furthermore, with increasing root crack level, the TVMS reduction rate in the first double-tooth

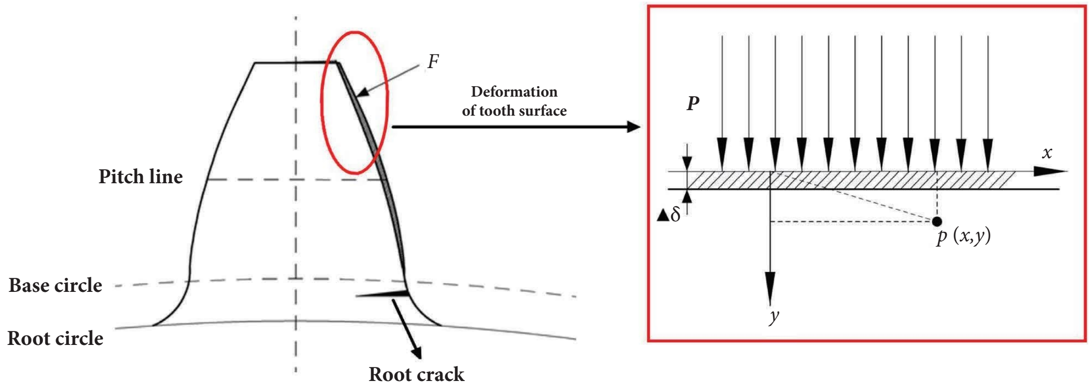

(a) (b)

FIGURE 5: Schematic of the oil film deformation of gear contact with lubrication: (a) single tooth deformation and (b) tooth surface deformation.

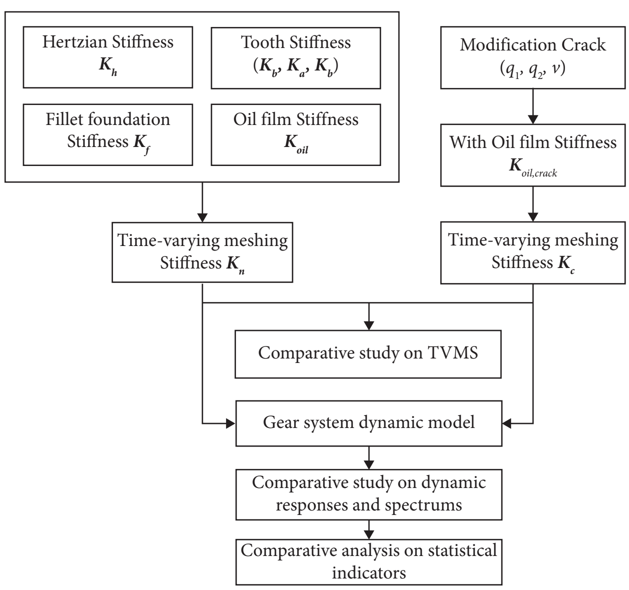

FIGURE 6: The research framework of the proposed method.

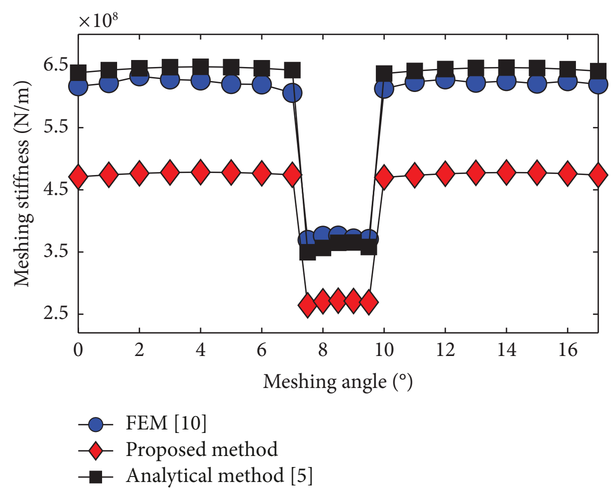

FIGURE 7: TVMS results of the proposed method and AM for health gear.

TABLE 1: The gear and lubricant parameters.

Description	Values
Normal module	2.5 mm
Number of teeth	37
Pressure angle	20°
Face width	20 mm
Young's modulus	206 GPa
Lubricant temperature	30°C
Poisson's ratio	0.3
Initial lubricant viscosity	0.08 Pa·s
Initial lubricant density	870 kg/m^3
Rotation speed	600 rpm
Surface sliding velocity	9 m/s

contact region is much higher than that in the second double-tooth contact region because the reduction part of inertia moment I_y and cross-sectional area A_y when the tooth root occurs crack in the first double-tooth contact region are higher than in the second double-tooth contact region. Therefore, it indicates that the TVMS of the oil film is also affected to the meshing region when the crack of the toot root happened.

4. Results of Vibration Analysis

To study the vibration feature of the cracked tooth considering the TVMS of oil film, this section has established a dynamic lumped model of a single-state gear system with 6-DOF, and the dynamic response of the cracked tooth is applied in which the dynamic parameter of the TVMS is estimated in Section 2 to find the failure mechanism of the cracked gear for analyzing time domain, frequency domain and statistical characteristic of vibration signal. The dynamic model adopts a classical 6-DOF gear meshing model which includes 2 rotation of moment inertias and 4 translational inertias for the pinion and gear, and Figure 12 evidence the 6-DOF dynamic model diagram.

The equation of dynamic motion with 2-rotational moments of inertia are given by

Table 2: Relative error of TVMS with different methods.

	Maximum stiffness of single contact/10^8 (N/m)	Relative error with ISO (%)	Average stiffness of total meshing/10^8 (N/m)	Relative error with ISO (%)
AM	3.6481	30.55	5.7605	28.32
FEM	3.7634	34.67	5.6241	25.28
Proposed method	2.7072	3.12	4.0618	9.51
ISO standard	2.7944	0	4.4891	0

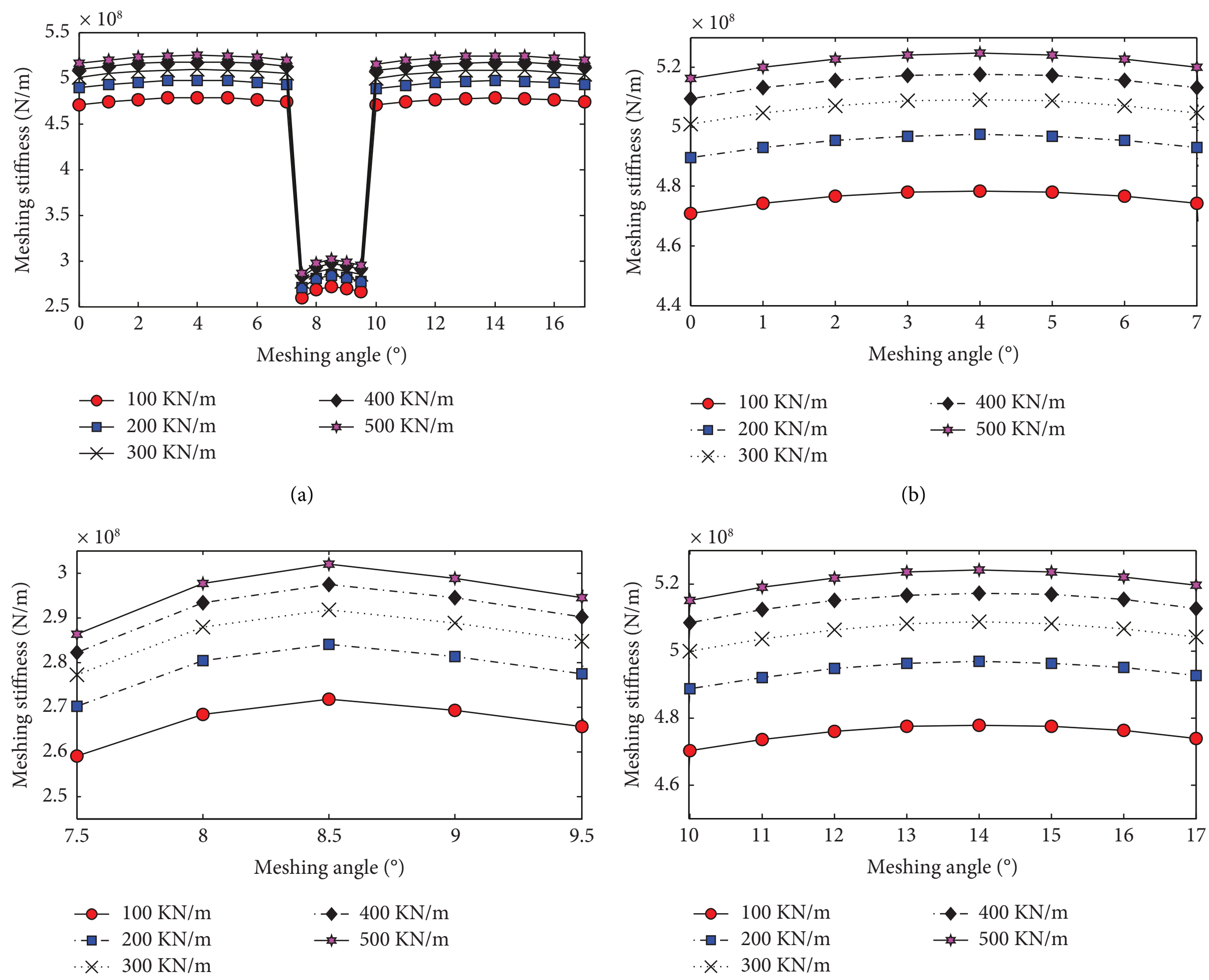

Figure 8: The TVMS result varies with different contact forces: (a) overall trend, (b) close-up of first double-tooth pairs, (c) close-up of single-tooth pairs, and (d) close-up of second double-tooth pairs.

$$
\begin{aligned}
I_p \frac{d^2\theta_p}{dt^2} - M_{pF_f} + M_{pF} &= T_p, \\
I_g \frac{d^2\theta_g}{dt^2} + M_{gF_f} - M_{gF} &= -T_g.
\end{aligned} \tag{25}
$$

For the x-axis direction, the equations of the 2-translational moment are as follows:

$$
\begin{aligned}
m_p \frac{d^2 x_p}{dt^2} + C_{px} \frac{dx_p}{dt} + K_{px} x_p &= F_f, \\
m_g \frac{d^2 x_g}{dt^2} + C_{gx} \frac{dx_g}{dt} + K_{gx} x_g &= -F_f.
\end{aligned} \tag{26}
$$

For the y-axis direction, the other 2-translational moments are as follows:

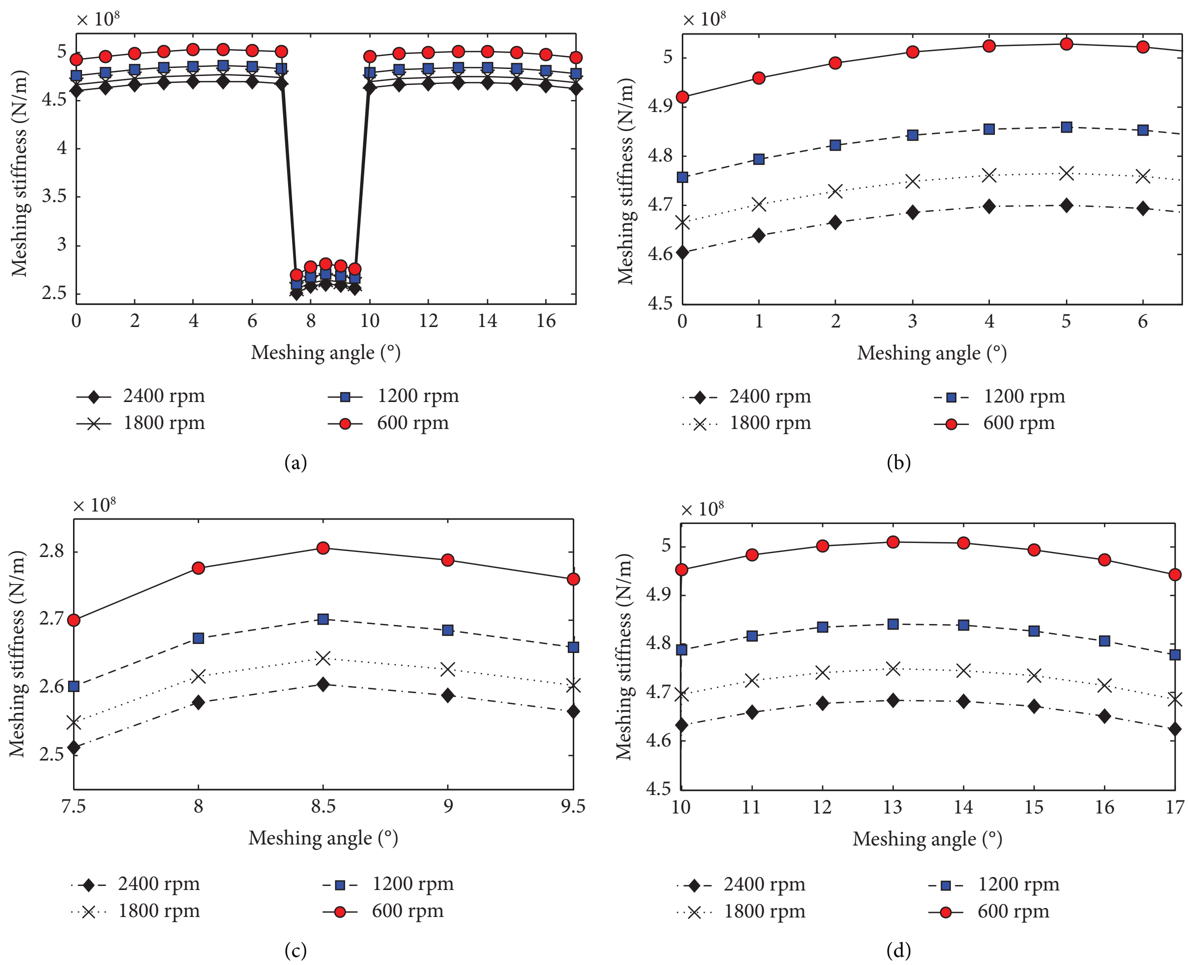

Figure 9: The TVMS result varies with different rotation speeds: (a) overall trend, (b) close-up of first double-tooth pairs, (c) close-up of single-tooth pairs, and (d) close-up of second double-tooth pairs.

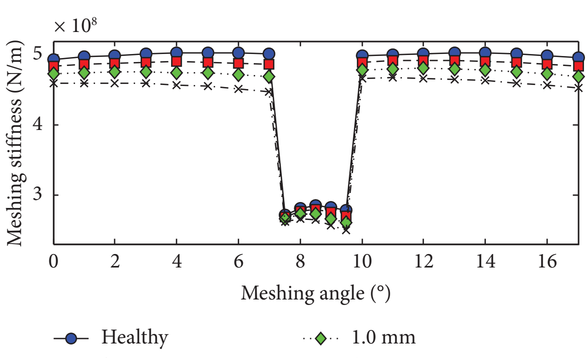

Figure 10: Comparison of TVMS for gear healthy and 3 cases of crack failure.

$$\begin{aligned} m_p \frac{\mathrm{d}^2 y_p}{\mathrm{d}t^2} + C_{py} \frac{\mathrm{d} y_p}{\mathrm{d}t} + K_{py} y_p &= F, \\ m_g \frac{\mathrm{d}^2 y_g}{\mathrm{d}t^2} + C_{gy} \frac{\mathrm{d} y_g}{\mathrm{d}t} + K_{gy} y_g &= -F, \end{aligned} \quad (27)$$

where I, m, C, and K denote the moment of inertia, mass, damping, and stiffness for dynamic system of gear pair, respectively, and the subscript p and g represent the pinion and gear, respectively. M_p and M_g are the moment induced by the contact force F and the friction force F_f, respectively [35]. The θ is the degree of angular rotation of the gear, and x and y are the transverse displacement along the x and y direction, respectively.

Considering TVMS and contact damping of gear pair, the dynamic mesh force F can be expressed as follows:

$$F = K_m(t)\left(\gamma_0 e_g(t) + \gamma_1 b_g\right) + C_m \gamma_0 \dot{e}_g(t), \quad (28)$$

where $K_m(t)$ is the total TVMS which obtained by (24), C_m is the contact damping, b_g is the half backlash of gear pair and $e_g(t)$ is the transmission error of gear pair which can be obtained as follows [7, 26]

$$e_g(t) = R_{bp}\theta_p - R_{bg}\theta_g + x_p - x_g, \quad (29)$$

where R_{bp} and R_{bg} are the radio of base circle for the pinion and gear, respectively, and the backlash function γ_0 and γ_1 are written as follows:

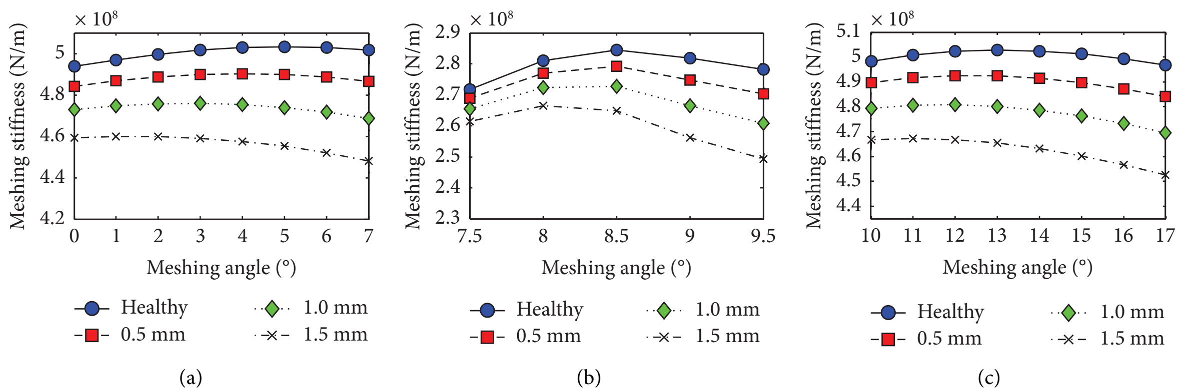

Figure 11: Enlarged view of TVMS in different meshing intervals: (a) first double-tooth, (b) single-tooth, and (c) second double-tooth.

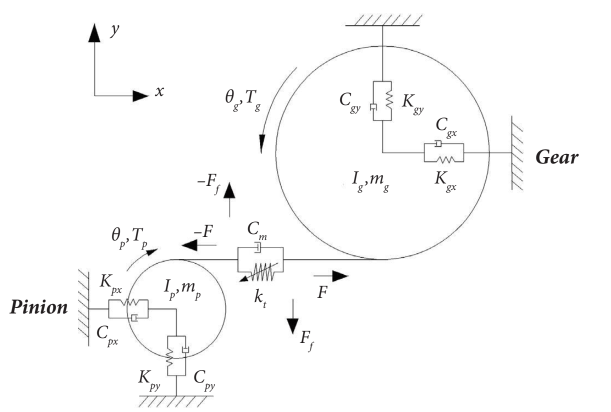

Figure 12: Dynamic model of single stage gear pair with 6 DOF.

$$\gamma_0 = \begin{cases} 1, & |e_g(t)| \geq b_g, \\ 0, & |e_g(t)| < b_g, \end{cases}$$
$$\gamma_1 = \begin{cases} -1, & e_g(t) \geq b_g, \\ 0, & |e_g(t)| < b_g, \\ 1, & e_g(t) < b_g. \end{cases} \quad (30)$$

Also, the friction force F_f of gear pair contact by using Coulomb's law can be expressed as follows:

$$F_f = \mu \cdot F, \quad (31)$$

where μ is the friction coefficient, which was chosen as an invariant constant in this paper.

To investigate the effect of crack defects on the vibration feature of dynamic response, the 3 cases corresponding to different crack depths of tooth root are considered, and the gear mesh stiffness which is about to put in dynamic model are shown in Figure 13. The TVMS of health teeth is tiled into a whole meshing cycle, while the TVMS of cracked teeth is substituted into the position of the fifth meshing tooth, and it is clear to observed the reduction of meshing stiffness for the cracked gear with 0.5 mm, 1.0 mm, and 1.5 mm, which hints at the significant variety in the vibration responses of tooth cracked defects.

The detailed parameters of the dynamic model with the gear pair are given in Table 3. Considering the TVMS of the gear pair shown in Figure 13 into the dynamic model, the vibration response of the 6-DOF dynamic model at the x-direction of the driven gear for 4 condition cases is extracted as shown in Figure 14. For the dynamic response of the healthy case, the time-domain response depicts the period motion of the smooth and steady meshing vibration, which coincides well with the TVMS of the one time period. With the presence of the cracked tooth root and the reduction of the TVMS on the fifth tooth, the cracked tooth meshes once per revolution. Therefore, it is clearly found that the response amplitude of the fifth tooth is supposed to appear as obviously impulse in the time domain of Figure 14, when the cracked tooth is in contact. The enlarged view in the time domain of the cracked response of 4 cases (in Figure 15) shows that the time interval between the three crack impulses is 0.0027 s, which is approximately equal to the meshing period of one tooth $T_s = 0.0027\,\text{s} = 1/f_{\text{m}}$, and it is also found that the region-A, region-B, and region-C from Figure 15 present the beginning engaged region of the first double-teeth contact, single-teeth contact, and second double-teeth contact, respectively, and also that of the region with a higher amplitude of impulse response by the cracked tooth. Furthermore, it is clearly seen that the impulse amplitude increases with the growth of the crack depth in the enlarged figures of regions A, B, and C.

Furthermore, considering that the root of the only cracked tooth is cracked, the modulation effect of the root crack occurs once per revolution, and the modulation frequency is usually the shaft frequency $f_s = 10\,\text{Hz}$ of the rotation shaft of the cracked tooth. Such modulation effect of rotation frequency can give rise to the sidebands around the mesh frequency in the spectrum, and the sideband frequency couples with the harmonics of the gear mesh frequency. Figures 16–22 present the spectrum/cepstrum of dynamic responses for health gear and 3 cracked cases.

In comparison between the health gear and 3 cracked depths for the dynamic response spectrum, the sideband of rotation frequency of cracked gear appears around the high-harmonic gear mesh frequency as shown in Figures 16–22, and the results of cepstrum analysis present several

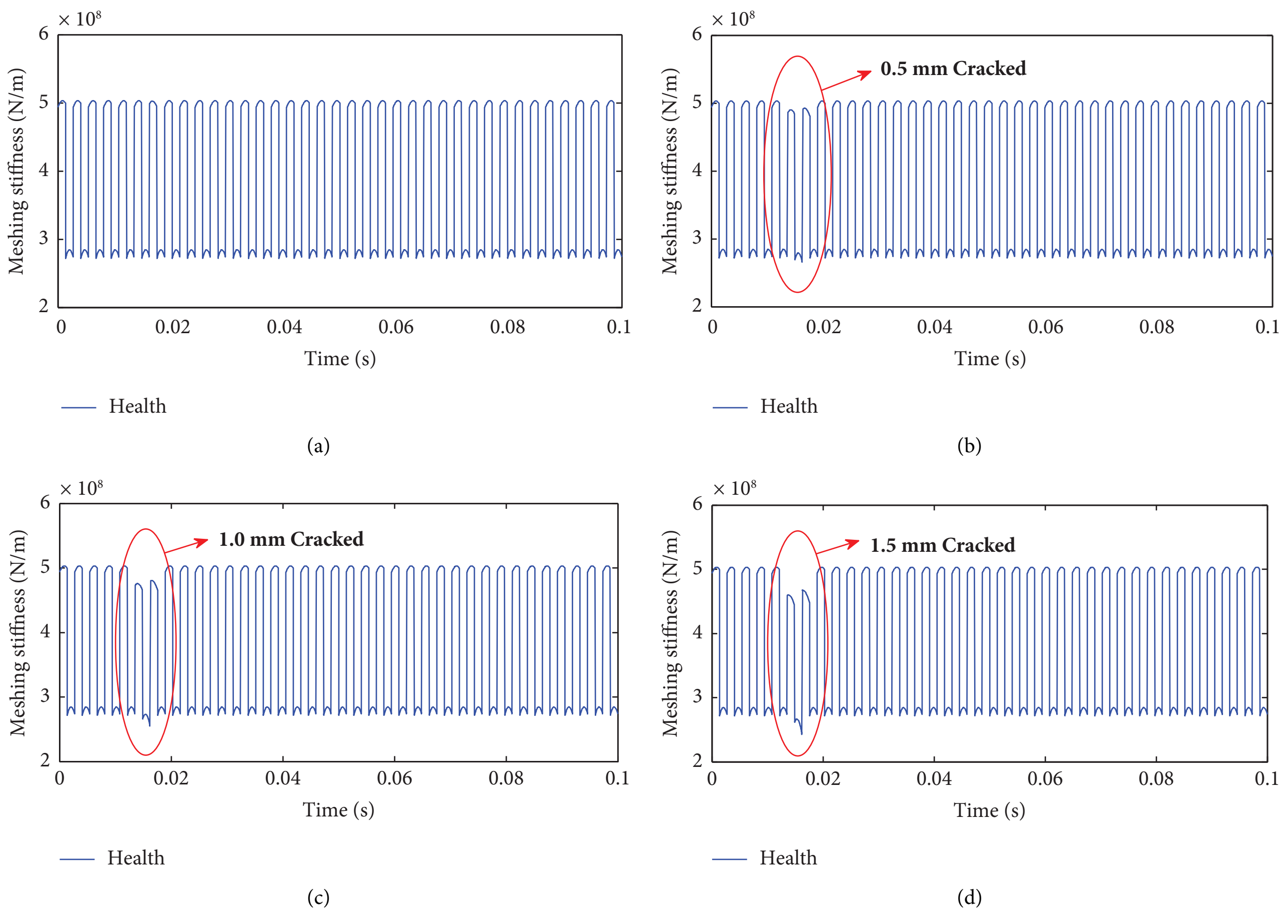

FIGURE 13: The TVMS in one rotation period for 4 cases of gear pair: (a) healthy gear, (b) 0.5 mm cracked, (c) 1.0 mm cracked, and (d) 1.5 mm cracked.

TABLE 3: The parameters used for dynamic modeling.

Description	Symbol	Parameters
Mass of pinion and gear	m_p, m_g	1.133 kg
Mass moment inertia of pinion and gear	I_p, I_g	2.813×10^{-3} kg·m^2
Radial stiffness of pinion and gear	$K_{px}, K_{gx}, K_{py}, K_{gy}$	6.56×10^8 N/m
Radial damping of pinion and gear	$C_{px}, C_{gx}, C_{py}, C_{gy}$	1.8×10^3 N·s/m
Torsional damping between meshing teeth	C_m	67
Friction coefficient of meshing teeth	μ	0.02
Time-varying meshing stiffness	$K_m(t)$	Given by Figure 13
Rotation speed of pinion	R_n	600 rpm

obviously periodic impulses in which the component scale of frequency is the drive shaft frequency f_s, and it is also found that there is a harmonic signal with a period of meshing frequency f_m bandwidth around a high-amplitude pulse whose period is the drive shaft frequency f_s. In conclusion, the amplitudes of the sideband in the frequency spectrum and the impulse amplitudes of the cepstrum increases with the cracked growth, respectively, as shown in Table 4.

For instance, the average amplitude of sideband, at healthy gear is 1.759×10^{-4}, while those at 0.5 mm cracked, 1.0 mm cracked and 1.5 mm cracked are 7.428×10^{-4}, 1.816×10^{-3}, and 3.461×10^{-3}, respectively, and the impulse amplitude of cepstrum at healthy gear, 0.5 mm, 1.0 mm, and 1.5 mm cracked are 0.1433, 0.3713, 0.4229, and 0.7237 respectively. This is because the vibration impulse at rotation frequency $f_s = 10$ Hz caused by the cracked tooth root gradually becomes the dominant element in the dynamic response, while internal excitations (meshing frequency) still play a dominant role in gear contact. In the depth range of root crack from 0.5 mm to 1.5 mm, the amplitude of the sideband frequency with a slight crack differs greatly from that of the severe root crack. Taking crack growth from 0.5 mm to 1.0 mm and 1.0 mm to 1.5 mm as an analysis, the average amplitude increments of sideband frequency are 0.012 and 0.02, respectively. Thus, the rotation frequency around the harmonic of meshing frequency is the main

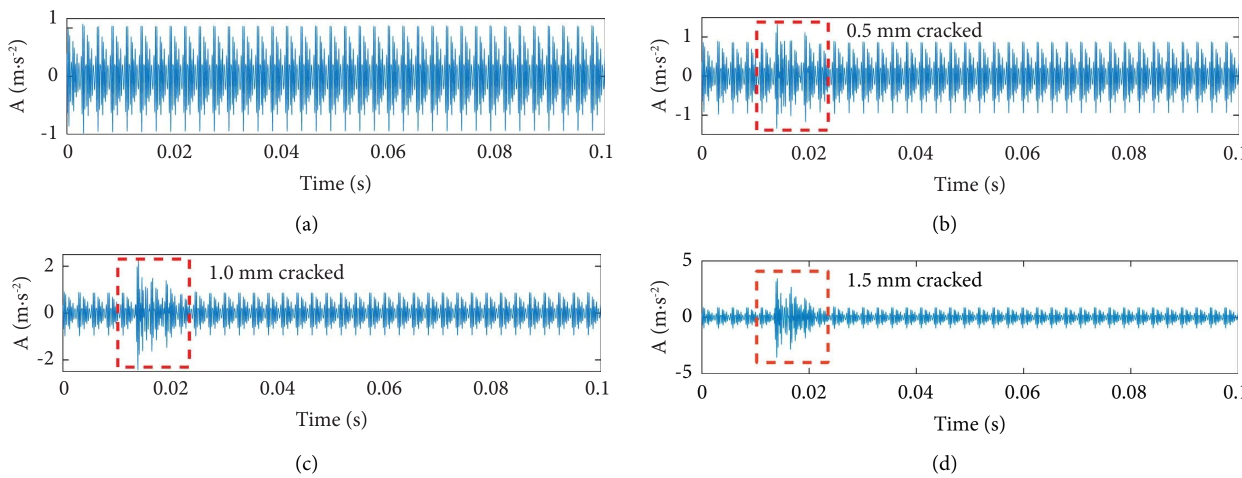

FIGURE 14: Dynamic responses of gear with x direction for the 4 cases: (a) healthy gear, (b) 0.5 mm cracked, (c) 1.0 mm cracked, and (d) 1.5 mm cracked.

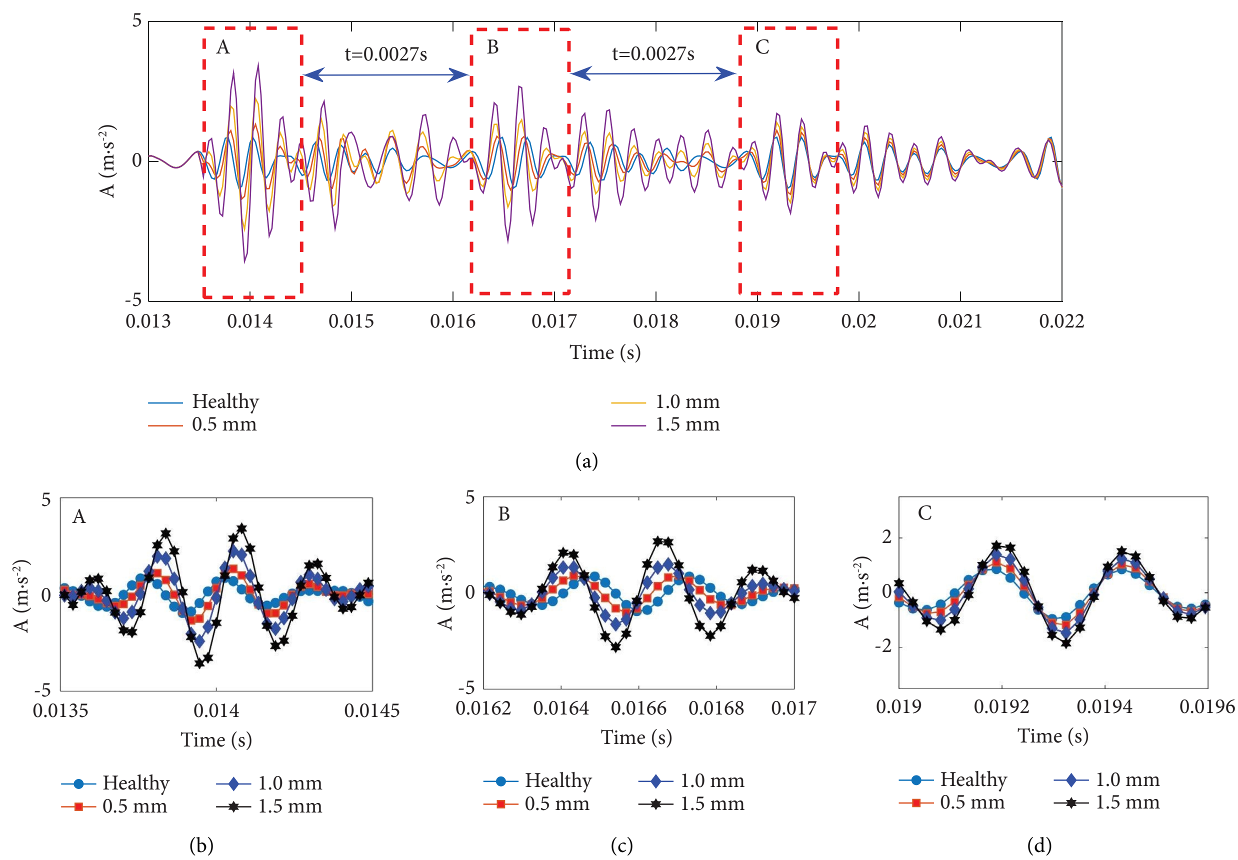

FIGURE 15: (a) Enlarged view of impulse region for dynamic responses, (b) enlarged view of region-A, (c) enlarged view of region-B, and (d) enlarged view of region-C.

monitoring component when the tooth root crack appears, and the rotation frequency at the spectrum has a significant determine on the failure detection of gear cracks.

As the gear pair appears to have a tooth root crack that can cause vibration variation in dynamic responses, the 4 vibration indicators are introduced to analyze the cracked gear of vibration feature and failure level. These characteristic indicators of signal analysis are the statistic statement based on the vibration characteristic of the dynamic response, including sideband ratio (SBR), kurtosis, root mean square (RMS), and frequency of root mean square (RMSF) [6, 21], and these indicators can be defined as follows:

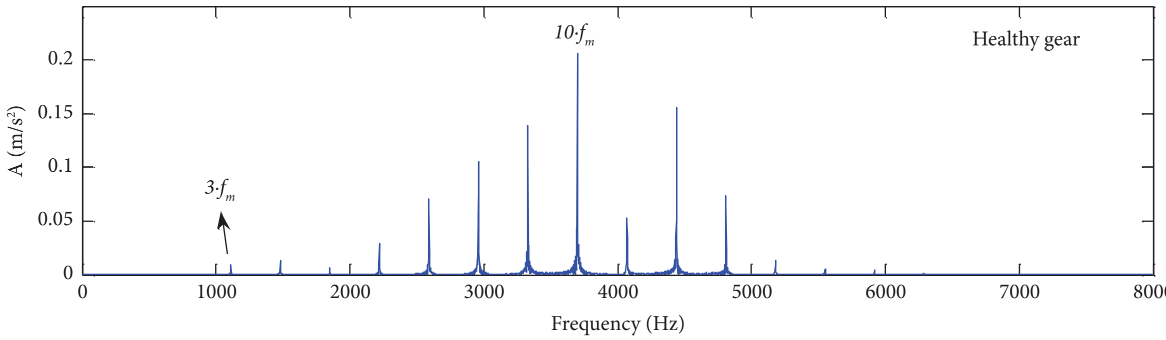

Figure 16: The frequency spectrum of the dynamic response with healthy gear.

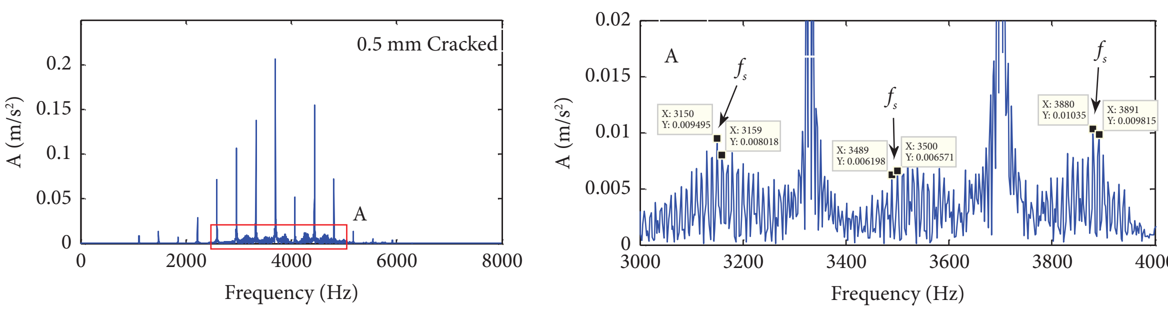

Figure 17: The frequency spectrum of dynamic response with the 0.5 mm cracked.

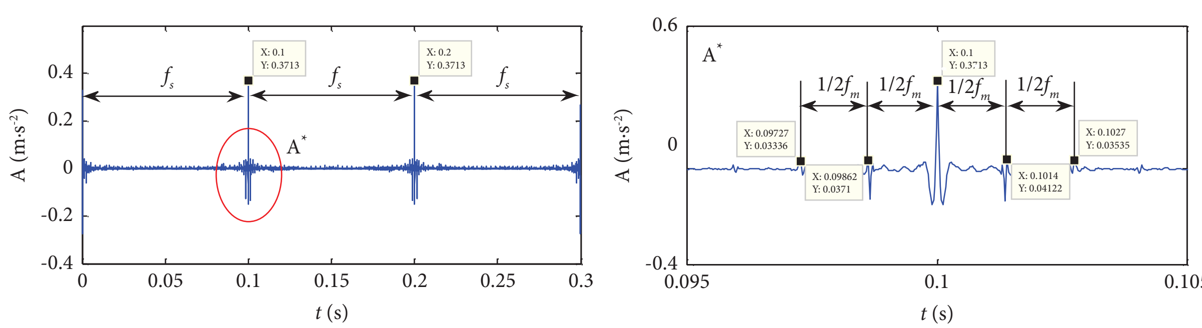

Figure 18: The frequency cepstrum of dynamic response with the 0.5 mm cracked.

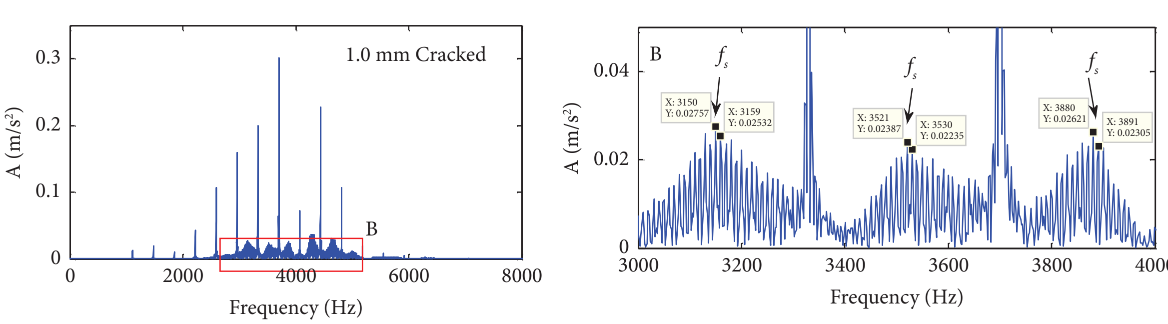

Figure 19: The frequency spectrum of dynamic response with the 1.0 mm cracked.

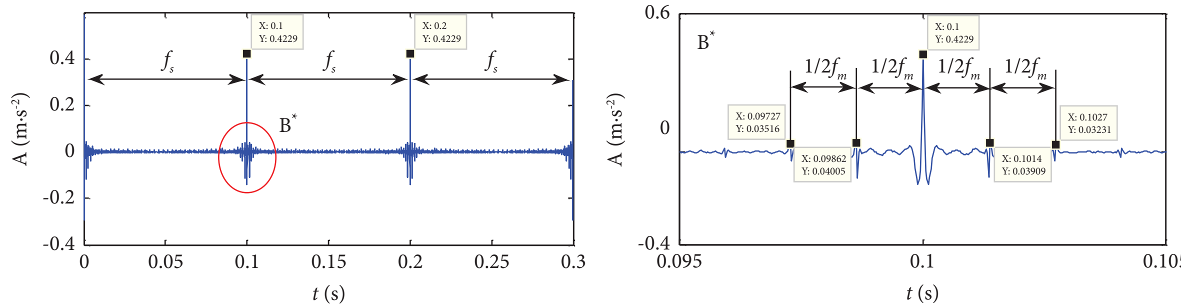

Figure 20: The frequency cepstrum of dynamic response with the 1.0 mm cracked.

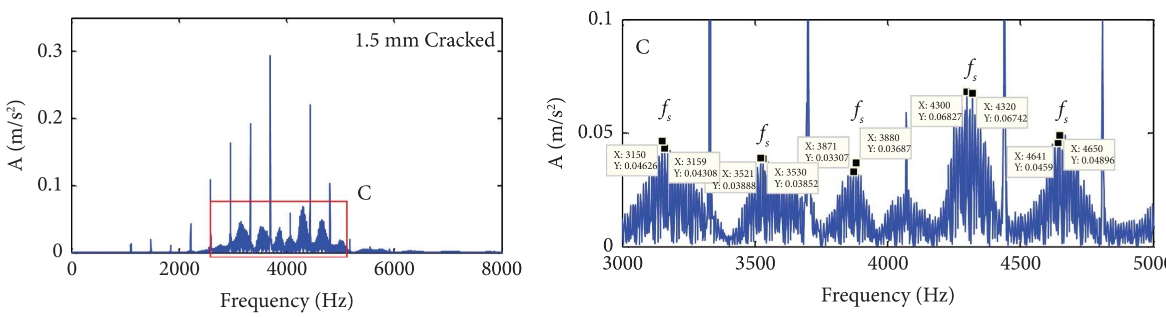

Figure 21: The frequency spectrum of dynamic response with the 1.5 mm cracked.

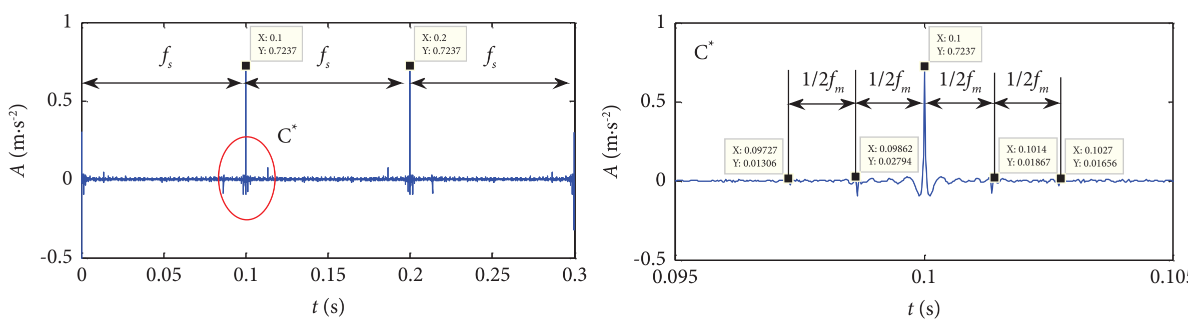

Figure 22: The frequency cepstrum of dynamic response with the 1.5 mm cracked.

Table 4: Comparison of the average amplitude of the sideband for healthy and 3 crack cases.

Cases	Average amplitude of sideband (m/s^2)	Relative increment with heathy gear (×100%)	Impulse amplitude of cepstrum (m/s^2)	Relative increment with heathy gear (×100%)
Healthy	0.001759	0	0.1433	0
0.5 mm	0.007428	3.22	0.3713	0.61
1.0 mm	0.018162	9.32	0.4229	1.95
1.5 mm	0.034619	18.68	0.7237	4.05

Table 5: Comparison of characteristic indicators for healthy and 3 crack cases.

Cases	Arithmetic value of indicators				Increment percent of indicators (×100%)			
	RMS	Kurtosis	RMSF	SBR	RMS	Kurtosis	RMSF	SBR
Healthy	0.3799	2.7312	0.1167	3.3490	0	0	0	0
0.5 mm	0.3882	2.8192	0.1317	5.3084	0.0219	0.0322	0.1288	0.5850
1.0 mm	0.4149	4.1933	0.1323	8.0368	0.0923	0.5353	0.1336	1.3997
1.5 mm	0.4743	8.8871	0.1387	12.0606	0.2485	2.2538	0.1889	2.6012

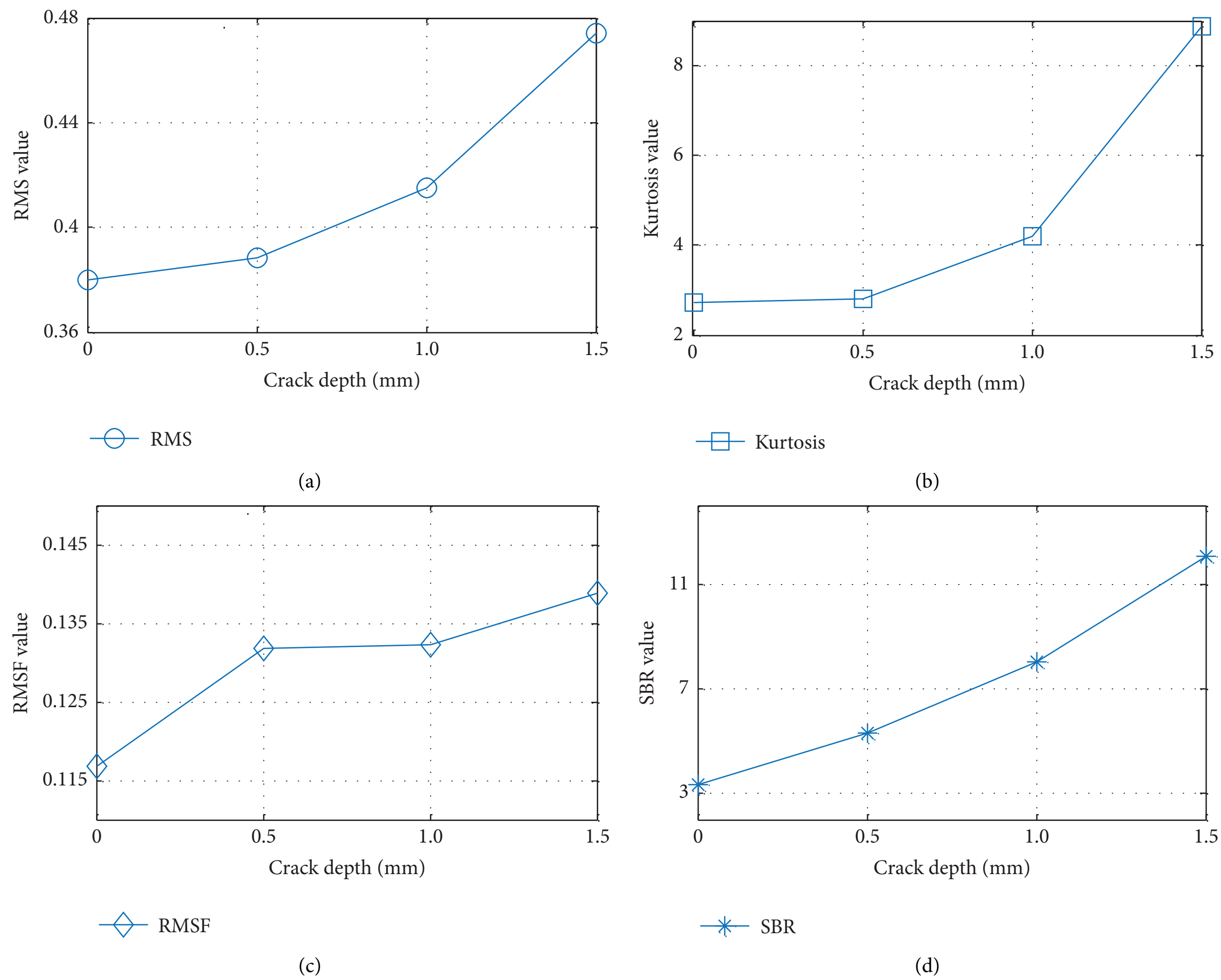

Figure 23: The indicator value is modified with different crack depths: (a) RMS, (b) Kurtosis, (c) RMSF, (d) SBR.

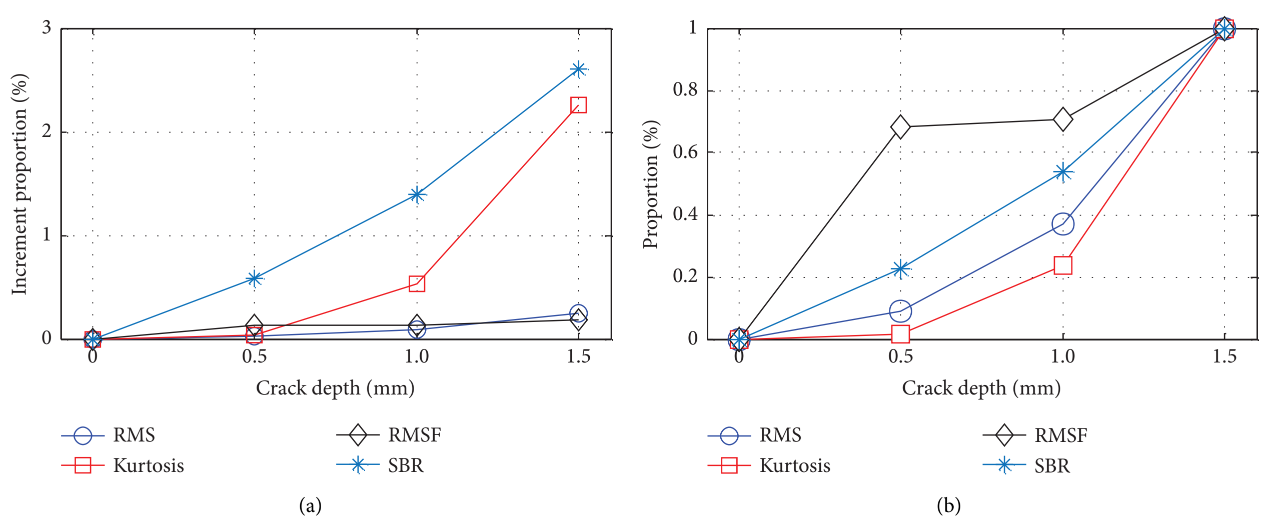

Figure 24: (a) Increment proportion of 4 indicators and (b) normalized proportion.

$$\mathrm{RMS} = \sqrt{\frac{1}{N}\sum_{n=1}^{N}\left(x(n)-\overline{x}\right)^2},$$

$$\mathrm{Kurtosis} = \frac{1/N\sum_{n=1}^{N}\left(x(n)-\overline{x}\right)^4}{\left[1/N\sum_{n=1}^{N}\left(x(n)-\overline{x}\right)^2\right]^2},$$

$$\mathrm{RMSF} = \sqrt{\frac{\sum_{n=1}^{N} f^2(n)s(n)}{\sum_{n=1}^{N} s(n)}}, \tag{32}$$

$$\mathrm{SBR} = \sum_{k=1}^{K}\frac{1}{f^2(k)}\sum_{n=1}^{N}\left|R_n\left(f_n\right)\right|^2,$$

where $x(n)$ is the signal series in the time-domain which $n = 1, 2, \ldots, N$, $s(n)$ is the spectrum line of $x(n)$, $f(k)$ is the amplitude of the harmonic of kth meshing $R_i(f_i)$ is the Fourier series spectrum of $x(n)$. The percent increment of the characteristic indicator is introduced to describe the vibration variation of the dynamic response for the cracked tooth root, expressed as follows:

$$I_{X_i} = \frac{X_i - X_{\mathrm{Healthy}}}{X_{\mathrm{Healthy}}} \times 100\%, \tag{33}$$

where X presents the characteristic indicator (RMS, Kurtosis, RMSF, and SBR), and the subscript i denotes the crack depth of 0.5 mm, 1.0 mm, and 1.5 mm.

The four typical feature indicators which can significantly reflect the effect of the vibration feature at the different crack depths are given in Table 5. From Figure 23, it is shown that these indicators modify with the increase in crack depth of tooth root, and the change trend of the indicators is gradually increasing. When the crack appears in an early failure such as 0.5 mm depth, the increment course of the indicator SBR is obvious that it is higher than 1.9593 and the percentage of increment of SBR is 0.5850 compared to healthy and 0.5 mm cracked. Therefore, the SBR feature is better than other indicators to detect cracks in the tooth root in the early stages of the defect. In Figure 24, the feature indicators are initialized incrementally and normalized to observe the detection mechanism for the indicator curve varying with the crack depth. RMS, Kurtosis, and SBR obviously increase even at the moderate stage of crack failure, and the increment percent of RMS, Kurtosis, and SBR at the 0.5 mm to 1.0 mm are 7.04%, 50.31%, and 81.47%, respectively, which demonstrate better detection in tooth root crack failure. But the incremental ratio of the RMSF performance is relatively poor detection, at only 0.48%. Differently in other crack stages, these 4 indicators are obviously sensitive in serious crack failure (1.5 mm) from Fig. 24(b), which increment percent of the 4 indicators is 13.62%, 171.85%, 5.53%, and 120.15%, respectively. Therefore, in the four cases of gear stage, all these indicators can reflect the variation principle of the crack failure, while these 3 indicators of RMS, Kurtosis, and SBR can efficiently detect the increase of crack failure for 1.0 mm and 1.5 mm, and the indicator of RMSF exhibits high sensitivity at early failure of a 0.5 mm crack due to the RMSF showing the average vibration amplitude in spectrum.

5. Conclusions

In this paper, an improved TVMS calculation model is proposed that considers oil film stiffness in EHL line contact for crack failure of the tooth root. This model employs the thickness of the oil film to estimate the elastic deformation of the oil film in gear contact, considering the variation in the profile of the oil film induced by the cracked tooth root. The TVMS result is calculated by combining the stiffness of the body contact and the contact of the oil film, and the overall result of the mesh stiffness of the proposed model decreases because of the stiffness of the oil film. The effect of the two parameters of work condition (rotation speed and contact force) of gear in the proposed model on the TVMS is also investigated. The TVMS of the oil film depends mainly on the rotation speed because the increase in rotation speed affects the oil film thickness, which is related to the stiffness of the oil film. Therefore, the TVMS decreases as the rotation speed is increased throughout the meshing period. And a 6-DOF dynamic model is produced to analyze the vibration behaviors using the calculated oil film TVMS. From the time-domain analysis, frequency-domain analysis, and statistical indicator analysis, the impulse amplitude of vibration response obviously increases when the crack depth increases, and the spectrum line of the sideband with the rotational frequency as the bandwidth appears around the harmonic of the meshing frequency.

Data Availability

Data availability is not applicable to this article as no new data were created or analyzed in this study.

Conflicts of Interest

The authors declare that they have no conflicts of interest.

Acknowledgments

This research was financially supported by the National Natural Science Foundation of China (Grant nos. 51875183 and 51975193) and the Research Foundation of Education Bureau of Hunan Province, China (Grant no. 22B0199).

References

[1] A. S. Mohamed, S. Sassi, and M. Roshun Paurobally, “Model-Based analysis of spur gears’ dynamic behavior in the presence of multiple cracks,” *Shock and Vibration*, vol. 2018, no. 4, Article ID 1913289, 20 pages, 2018.

[2] Y. Luo, N. Baddour, and M. Liang, “Dynamical modeling and experimental validation for tooth pitting and spalling in spur gears,” *Mechanical Systems and Signal Processing*, vol. 119, pp. 155–181, 2019.

[3] F. Chaari, T. Fakhfakh, and M. Haddar, “Analytical modelling of spur gear tooth crack and influence on gearmesh stiffness,”

European Journal of Mechanics- A: Solids, vol. 28, no. 3, pp. 461–468, 2009.
[4] N. I. Muskhelishvili, *Some Basic Problems of The Mathematical Theory Of Elasticity*, vol. 4, Springer, Dordrecht, Netherlands, 2019.
[5] Z. Chen, Z. Zhou, W. Zhai, and K. Wang, "Improved analytical calculation model of spur gear mesh excitations with tooth profile deviations," *Mechanism and Machine Theory*, vol. 149, Article ID 103838, 2020.
[6] J. Ning, Z. Chen, Y. Wang, Y. Li, and W. Zhai, "Vibration feature of spur gear transmission with non-uniform depth distribution of tooth root crack along tooth width," *Engineering Failure Analysis*, vol. 129, Article ID 105713, 2021.
[7] V. Kumar, A. Kumar, S. Kumar, and S. Sarangi, "TVMS calculation and dynamic analysis of carburized spur gear pair," *Mechanical Systems and Signal Processing*, vol. 166, Article ID 108436, 2022.
[8] Z. Shen, B. Qiao, L. Yang, W. Luo, and X. Chen, "Evaluating the influence of tooth surface wear on TVMS of planetary gear set," *Mechanism and Machine Theory*, vol. 136, pp. 206–223, 2019.
[9] A. Flodin and S. Andersson, "Simulation of mild wear in spur gears," *Wear*, vol. 207, no. 1-2, pp. 16–23, 1997.
[10] J. Wang, J. Yang, Y. Lin, and Y. He, "Analytical investigation of profile shifts on the mesh stiffness and dynamic characteristics of spur gears," *Mechanism and Machine Theory*, vol. 167, Article ID 104529, 2022.
[11] X. Wu, Y. Luo, Q. Li, and J. Shi, "A new analytical model for evaluating the time-varying mesh stiffness of helical gears in healthy and spalling cases," *Engineering Failure Analysis*, vol. 131, Article ID 105842, 2022.
[12] W. J. Chung, J. H Park, H. G. Yoo et al., "Improved analytical model for calculating mesh stiffness and transmission error of helical gears considering trochoidal root profile," *Mechanism and Machine Theory*, vol. 163, Article ID 104386, 2021.
[13] Y. Yang, N. Hu, J. Tang, J. Hu, L. Zhang, and Z. Cheng, "Dynamic analysis for a spur geared rotor system with tooth tip chipping based on an improved time-varying mesh stiffness model," *Mechanism and Machine Theory*, vol. 165, Article ID 104435, 2021.
[14] I. V. Singh, B. K. Mishra, S. Bhattacharya, and R. U. Patil, "The numerical simulation of fatigue crack growth using extended finite element method," *International Journal of Fatigue*, vol. 36, no. 1, pp. 109–119, 2012.
[15] J. Zhan, M. Fard, and R. Jazar, "A CAD-FEM-QSA integration technique for determining the time-varying meshing stiffness of gear pairs," *Measurement*, vol. 100, pp. 139–149, 2017.
[16] J. G. Verma, S. Kumar, and P. K. Kankar, "Crack growth modeling in spur gear tooth and its effect on mesh stiffness using extended finite element method," *Engineering Failure Analysis*, vol. 94, pp. 109–120, 2018.
[17] S. Yanning, M. Hui, H. F. Yifan, C. Kangkang, C. Liuyang, and W. Bangchun, "A revised time-varying mesh stiffness model of spur gear pairs with tooth modifications," *Mechanism and Machine Theory*, vol. 129, pp. 261–278, 2018.
[18] Q. Wang, B. Zhao, Y. Fu, X. Kong, and H. Ma, "An improved time-varying mesh stiffness model for helical gear pairs considering axial mesh force component," *Mechanical Systems and Signal Processing*, vol. 106, pp. 413–429, 2018.
[19] H. Ma, R. Song, X. Pang, and B. Wen, "Time-varying mesh stiffness calculation of cracked spur gears," *Engineering Failure Analysis*, vol. 44, pp. 179–194, 2014.
[20] X. Liang, H. Zhang, M. Zuo, and Y. Qin, "Three new models for evaluation of standard involute spur gear mesh stiffness," *Mechanical Systems and Signal Processing*, vol. 101, pp. 424–434, 2018.
[21] X. Liang, M. J. Zuo, and Z. Feng, "Dynamic modeling of gearbox faults: a review," *Mechanical Systems and Signal Processing*, vol. 98, pp. 852–876, 2018.
[22] Y. Pandya and A. Parey, "Experimental investigation of spur gear tooth mesh stiffness in the presence of crack using photoelasticity technique," *Engineering Failure Analysis*, vol. 34, pp. 488–500, 2013.
[23] F. Karpat, C. Yuce, and O. Doğan, "Experimental measurement and numerical validation of single tooth stiffness for involute spur gears," *Measurement*, vol. 150, Article ID 107043, 2020.
[24] S. S. Patil, S. Karuppanan, and I. Atanasovska, "Experimental measurement of strain and stress state at the contacting helical gear pairs," *Measurement*, vol. 82, pp. 313–322, 2016.
[25] N. K. Raghuwanshi and A. Parey, "Experimental measurement of gear mesh stiffness of cracked spur gear by strain gauge technique," *Measurement*, vol. 86, pp. 266–275, 2016.
[26] J. Wu, Y. Yang, P. Wang, J. Wang, and J. Cheng, "A novel method for gear crack fault diagnosis using improved analytical-FE and strain measurement," *Measurement*, vol. 163, Article ID 107936, 2020.
[27] W. Qin, J. Chao, and L. Duan, "Study on stiffness of elastohydrodynamic line contact," *Mechanism and Machine Theory*, vol. 86, pp. 36–47, 2015.
[28] X. Zhang, H. Wu, C. Chen, D. Wang, and S. Li, "Oil film lubrication state analysis of piston pair in piston pump based on coupling characteristics of the fluid thermal structure," *Engineering Failure Analysis*, vol. 140, Article ID 106521, 2022.
[29] Y. Zhang, H. Liu, C. Zhu, M. Liu, and C. Song, "Oil film stiffness and damping in an elastohydrodynamic lubrication line contact-vibration," *Journal of Mechanical Science and Technology*, vol. 30, no. 7, pp. 3031–3039, 2016.
[30] Y. Zhang, H. Liu, C. Zhu, C. Song, and Z. Li, "Influence of lubrication starvation and surface waviness on the oil film stiffness of elastohydrodynamic lubrication line contact," *Journal of Vibration and Control*, vol. 24, no. 5, pp. 924–936, 2018.
[31] C. Zhou, Z. Xiao, S. Chen, and X. Han, "Normal and tangential oil film stiffness of modified spur gear with non-Newtonian elastohydrodynamic lubrication," *Tribology International*, vol. 109, pp. 319–327, 2017.
[32] C. Zhou and Z. Xiao, "Stiffness and damping models for the oil film in line contact elastohydrodynamic lubrication and applications in the gear drive," *Applied Mathematical Modelling*, vol. 61, pp. 634–649, 2018.
[33] B. Hu, C. Zhou, and S. Chen, "Elastic dynamics modelling and analysis for a valve train including oil film stiffness and dry contact stiffness," *Mechanism and Machine Theory*, vol. 131, pp. 33–47, 2019.
[34] D. Dowson and G. R. Higginson, "A numerical solution to the elasto-hydrodynamic problem," *Journal of Mechanical Engineering Science*, vol. 1, pp. 6–15, 2006.
[35] S. He, S. Cho, and R. Singh, "Prediction of dynamic friction forces in spur gears using alternate sliding friction formulations," *Journal of Sound and Vibration*, vol. 309, no. 3-5, pp. 843–851, 2008.